Chemical Engineering Journal 154 (2009) 2–8

Contents lists available at ScienceDirect

Chemical Engineering Journal

journal homepage: www.elsevier.com/locate/cej

Transient isotopic kinetics study to investigate reaction mechanisms

B.S. Bal'zhinimaev*, E.M. Sadovskaya, A.P. Suknev

Boreskov Institute of Catalysis, pr. Lavrentieva, 5, 630090 Novosibirsk, Russia

ARTICLE INFO

Article history:
Received 27 November 2008
Received in revised form 23 March 2009
Accepted 11 April 2009

Keywords:
Isotope responses
Reaction mechanism
SSITKA
Ethylene epoxidation
Silver
NO reduction
Co-ZSM-5
Mass transfer
Fiberglass catalyst

ABSTRACT

This overview includes discussion of the principles, experimental and theoretical features of the isotopic transient kinetics for the study of reaction mechanism and evaluation of kinetic parameters. The results of the mechanistic study of ethylene epoxidation over silver, selective NO reduction with methane over Co-ZSM-5 and fiberglass based catalysts are presented. Investigation of ^{18}O isotope transfer dynamics allowed to reveal the reaction pathways towards ethylene oxide and CO_2 formation as well as to estimate the concentrations of active oxygen species and reaction rate coefficients of key steps. It was found that both ethylene epoxidation and deep oxidation proceed very fast in the microsecond range. A detailed SSITKA study of the NO reduction with methane using ^{15}N, ^{13}C and ^{18}O labels showed that reaction occurred via two parallel pathways involving in nitrite–nitrate and $NO_2^{\delta+}$ species, the last ones being 20 times more reactive. For the first time a transient isotopic kinetic study was used for evaluation of mass transfer parameters by an example of NO and water diffusion into the bulk of Pt-containing fiberglass catalyst.

1. Introduction

Study of the dynamics of isotope transfer under steady-state reaction conditions, the so-called Steady-State Isotopic Transient Kinetic Analysis (SSITKA), is successfully employed in investigation of the mechanism of catalytic reactions [1–6]. In distinction to the conventional transient response technique [7–10] we change stepwise not chemical composition of feed gas but the isotope one and record the dynamics of label transfer from reactants to reaction products. Obviously, at steady state and in the absence of kinetic isotope effects, the surface composition of adsorbed layer also remains unchanged at isotope replacement. Therefore, the observed isotope transients reflect only the features of reaction pathways and serve as "fingerprints" for reaction mechanism. In other words, SSITKA allows one to study the sequence of surface chemical reactions (steps) caused by breaking and formation of chemical bonds in reacting molecules.

In the case of stepwise disturbing of the feed gas chemical composition, the pattern of approaching a new steady state is governed not only by chemical (catalytic) steps, but also by various side processes, mostly of physical origin (phase transition, diffusion, etc.). These processes change the catalyst state and strongly complicate the revealing of reaction mechanism because they generally affect the reaction rate.

Historically the isotope techniques came into use in catalysis in 1960s [11] for evaluation of oxygen and other molecules reactivity. As a result, a lot of phenomena were discovered at that period. One of them is so-called "adsorption-assisted desorption", which implies that the desorption rate substantially depends on pressure of the adsorbing molecules [12]. The isotope techniques developed at that period have a disadvantage: they can be used in closed (static) systems, i.e. for the study of reversible reactions only.

Unlike closed systems, open systems allow studying both the reversible and irreversible catalytic reactions. This overview is devoted to experimental and theoretical aspects of SSITKA, its potentiality in identifying (discrimination) of reaction mechanism. A few examples of SSITKA application in the mechanistic study of ethylene epoxidation over silver, SCR of NO with methane over Co-ZSM-5, and NO and water reactions accompanyed by their mass transfer into the bulk of fiberglass based catalysts are presented.

2. SSITKA experimental

The basic idea of the isotope dynamic experiment is as follows. When reaction under study achieves steady state, the initial feed gas flow is stepwise replaced with another flow differing in the isotope composition, but absolutely identical in a chemical one (Fig. 1). The feed gas replacement is carried out by a fast 4-way valve with pneumatic drive, providing stepwise switching for 0.1 s.

The composition of feed gas and reaction products is continuously measured using a quadrupole mass spectrometer with computer acquisition, which makes it possible to analyze with

* Corresponding author. Tel.: +7 383 330 97 70 fax: +7 383 330 80 56.
E-mail address: balzh@catalysis.ru (B.S. Bal'zhinimaev).

1385-8947/$ – see front matter © 2009 Elsevier B.V. All rights reserved.
doi:10.1016/j.cej.2009.04.035

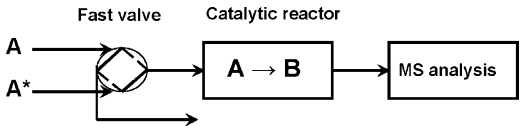

Fig. 1. Basic scheme of a SSITKA setup.

high time resolution a multicomponent reaction mixture of complex chemical and isotope composition. The experimental aspects of transient isotopic study are described in detail elsewhere [6]. The most important thing in SSITKA studies is a selection of reactor type. There are plug-flow and CSTR types of reactors, which differ in mass transfer regime. The decisive advantage of CSTR is that reaction takes place under gradientless conditions, which considerably simplifies the kinetic model. However, rather high response time of gas mixing in the reactor volume may distort the true dynamics of label transfer from reactants to reaction products.

Unlike CSTR, the SSITKA studies in a plug-flow reactor allow one to reveal more clearly a transient behavior of the catalyst surface. Most authors recommend that such studies are performed at low conversions in order to avoid gradients of concentration and temperature along catalyst bed. On the other hand, the lower is the conversion, the higher is the error in measuring of reaction products concentrations, and especially the fractions of different isotopes in these products. In this connection, we tried to estimate how vigorous are the constraints on conversion in plug-flow reactor for revealing the reaction mechanism by SSITKA.

As shown below, under the differential conditions, a time dependence of isotope fraction in the reaction product is the sum of exponents where their arguments are determined by a ratio of reaction rate to the concentration of intermediate species. In a plug-flow reactor the feed gas concentration decreases along the catalyst bed and, as a sequence the reaction rate (r) and the concentration of intermediates (θ) decrease also. However, their ratio changes in a relatively narrow range, and depends on order of reaction steps by intermediate species. In the case of the first-order kinetics ($r = k\theta$) this ratio is obviously constant. Accordingly the dynamics of isotope response does not depend on the reagents concentration profile along catalyst bed at all. In case of second-order kinetics this ratio changes slightly along catalyst bed, but significantly less than reagent concentration. The numerical analysis of different second-order kinetics showed clearly that at conversions up to 50% the $r = k\theta^2$ ratio changes within 15% from mean ratio (averaged along the reactor length). In this case the distinction of isotope responses calculated with regard to true $r(\xi)$ and $\theta(\xi)$ dependencies does not exceed a few percents only in comparison with averaged ones. Regarding higher order reactions they are not typical for gas phase reactions on solid catalysts.

Thus, taking into account the approximate model of plug-flow reactor (r = const, θ = const) we are able to determine quite reliably the most probable ways of isotope label transfer and estimate the integral values of concentrations for intermediate species in a wide range of conversions.

As for possible temperature gradients along the catalyst bed, they can be minimized using a 'single-row' Temkin reactor. In such reactors, catalyst beds alternate with the beds of inert heat carrier, so that each of the catalyst beds is actually a differential reactor. The inert beds serve for removing of heat in case of exothermic reaction. It is obviously, the higher is adiabatic heat, the more is number of alternating beds.

3. Discrimination of reaction mechanisms

As under steady state the rates of all reaction steps are constant, isotope label transfer from one compound to another occurs also at a constant rate and can be considered as first-order reaction with respect to isotope fraction. To reveal the features of isotope response caused by the reaction mechanism itself, assume that the reaction proceeds under differential conditions. Then a change in the isotope fraction in intermediate species on the catalyst surface is described by the linear Eq. (1):

$$\theta_k^{st}\frac{dZ_k^{\theta}}{dt} = \sum_{i=1}^{N_k^{\theta}} \gamma_i r_i^{st} Z_j \quad \text{Initial conditions: at } t = 0 \quad Z_i = Z^0, \tag{1}$$

and time dependence of isotopic fraction in the reaction product at $Z_A = 1$ can be expressed as:

$$Z_B(t) = \sum_{i=1}^{N} A_i \exp\left(-\frac{1}{\tau_{surfi}}t\right) + c \tag{2}$$

Here θ_k^{st} and Z_k^{θ} are respectively the steady-state concentrations of surface species and the relative label concentrations (isotope fractions) in them; r_i^{st} is the rate of a chemical reaction step; γ_i is the number of label atoms transferring from one substance to another in elementary reaction step (an analogue of stoichiometric coefficient), and $\tau_{surfi} = \theta_i^{st}/r_i^{st}$ is the surface-residence time of i-th intermediate species.

For simplest basic reaction pathways A → B (θ_i—intermediates), Eq. (1) is solved analytically. In the case of scheme I, the solution $Z_B(t)$ represents a simple exponential dependence, for consecutive steps (scheme II) – a difference of exponents, for schemes III and IV – the sum of exponents (Fig. 2a), and consecutive steps with a buffer one (V) are a superposition of schemes II and IV. Features of isotope responses for these mechanisms are more distinguishable on a logarithmic scale (Fig. 2b). In the first case the dependence is strictly

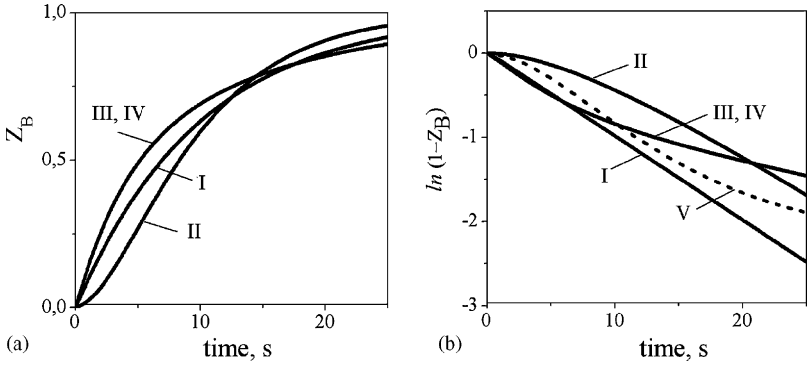

Fig. 2. Time dependencies of the linear (a) and logarithmic (b) isotope fractions in the reaction product for different types of reaction mechanisms.

linear, in the case of scheme II corresponding curves are always convex up; the convex down curves are intrinsic in schemes III and IV, while S-like shaped isotope response is observed for scheme V [13].

I) A → [θ1] → B

II) A → [θ1] → [θ2] → B

III) A → [θ1] → B, A → [θ2] → B

IV) A → [θ1] → B, [θ1] ⇄ [θ2]

V) A → [θ1] → [θ3] → B, [θ1] ⇄ [θ2]

The evaluation of Eq. (1) for various multistep reaction mechanisms shows that their identification is not limited basically by the number of steps. However, in some cases, a reaction mechanism cannot be specified. For example, schemes Va and Vb (differing in the position of buffer step in the consecutive mechanism) cannot be distinguished by only B isotope response:

Va) A → [θ1] → [θ3] → B, [θ1] ⇄ [θ2]

Vb) A → [θ1] → [θ3] → B, [θ3] ⇄ [θ2]

Nevertheless, if any reaction product (containing the same isotope label) desorbs at intermediate step (from θ_1 or θ_2), joint evaluation of isotope responses for both products simplifies discrimination of the reaction mechanisms. In particular, as it will be shown for ethylene epoxidation on silver, the analysis of ^{18}O transfer to both CO_2 and C_2H_4O allows one to distinguish the reaction pathway Va from Vb and make certain conclusions about reversibility of the steps.

Let us consider how the isotope response characteristics of each mechanism depend on type of the reactor. Isotope label transfer in CSTR is described by the following differential equations:

$$C_k^{st}\frac{dZ_k^C}{dt} = \frac{1}{\tau_g}(Z_k^{inlet}C_k^{inlet} - Z_kC_k^{st}) + \beta\sum_{i=1}^{N_k^C}\gamma_i r_i^{st}Z_j$$
$$\theta_k^{st}\frac{dZ_k^\theta}{dt} = \sum_{i=1}^{N_k^\theta}\gamma_i r_i^{st}Z_j \qquad (3)$$

Initial conditions: at $t = 0 \quad Z_j = Z^0$.

Here, C_k^{st} is the steady-state concentration of gases, $\tau_g = V/U$ is the gas phase residence time, β is dimensionless coefficient equal to $L{\cdot}W/V{\cdot}N_A$, where V is the r volume [cm^3], U is the volume flow rate [cm^3/s], L is the number of active sites per gram of catalyst [mol/g], W is the catalyst weight [g], and N_A is the number of gas molecules per unit volume [mol/cm^3].

Additional dynamic terms related to gas stirring in the reactor appear in the solution of Eq. (3). This leads to erasing of characteristic features of isotope responses peculiar to a definite reaction mechanism (Fig. 3), especially with an increase in the gas phase residence time. When τ_g is more or comparable with the surface-residence time, the reaction mechanisms become practically undistinguishable.

The process of isotope transfer in a plug-flow reactor is described by the differential equations in partial derivatives considering the change of isotope fraction both with time and along the catalyst bed (reactor length):

$$\frac{\partial C_k^{st}Z_k^C}{\partial t} + \frac{1}{\tau_g}\frac{\partial C_k^{st}Z_k^C}{\partial \xi} = \beta\sum_{i=1}^{N_k^C}\gamma_i r_i^{st}Z_j$$
$$\theta_k^{st}\frac{\partial Z_k^\theta}{\partial t} = \sum_{i=1}^{N_k^\theta}\gamma_i r_i^{st}Z_j \qquad (4)$$

Initial and boundary conditions: at $t = 0 \quad Z_j = Z^0$, at $\xi = 0 \quad Z_j = Z_j^{inlet}$.

In this case, the isotope responses virtually coincide with those calculated by idealized model (1), only a shift in time is observed (Fig. 4). This allows discriminating various reaction mechanisms in a wide range of τ_g values.

Numerical analysis includes the solution of inverse problem within a specified reaction mechanism to estimate the concentration of intermediate species and the rates of reaction steps in order to fit the experimental isotope responses. Note that SSITKA allows one to estimate without any modeling (simply from material balance) the total surface coverage or concentration of the active intermediates associated to a given isotope [4,14].

A set of values of the reaction step rates (r_i^{st}) at various steady-state concentrations of gases (C_i^{st}) and surface species (θ_i^{st}), obtained at variation of reactants concentration and temperature, allows one to define kinetic expressions for the rates of steps $r_i = k_i f_i(C,\theta)$ as well as to estimate the rate coefficients and activation energies. The principal difference of SSITKA from the conventional transient response technique implies that direct estimation of the concentration of active reaction intermediates is possible, which practically excludes a correlation

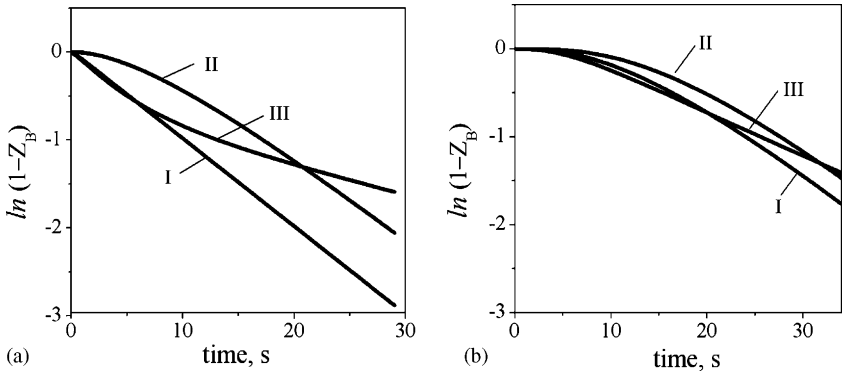

Fig. 3. Time dependencies of the logarithmic isotope fraction in the reaction product for different types of reaction mechanisms in CSTR at $\tau_g \ll \tau_{surf}$ (a) and $\tau_g \approx \tau_{surf}$ (b).

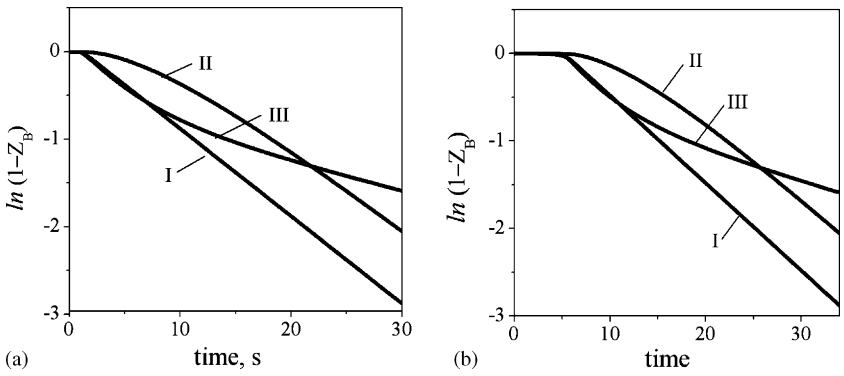

Fig. 4. Time dependencies of the logarithmic isotope fraction in the reaction product for different types of reaction mechanisms in a plug-flow reactor at $\tau_g \ll \tau_{surf}$ (a) and $\tau_g \approx \tau_{surf}$ (b).

between the values of kinetic parameters (coverages and rate coefficients).

4. SSITKA application for identification of reaction mechanism

4.1. Ethylene epoxidation on silver powder

The SSITKA studies of ethylene epoxidation on silver powder were performed in a flow setup with gradientless reactor [5,13]. Time dependencies of labeled reaction products (C_2H_4O and CO_2) were registered after stepwise replacement of $^{16}O_2$ with $^{18}O_2$ and vice versa in the feed gas (Fig. 5).

The logarithmic time dependence of ^{18}O fraction in carbon dioxide $\ln(1 - Z_{CO_2})$ (see inset on Fig. 5) is convex down, which is characteristic for the mechanism with a buffer step or with parallel ones. Since total amount of the substituted oxygen in CO_2 and H_2O exceeds considerably a monolayer coverage, we consider subsurface oxygen as one of intermediate species, which likely plays a role of buffer during isotope label transfer.

The logarithmic time dependence of ^{18}O fraction in ethylene oxide, $\ln(1 - Z_{C_2H_4O})$, is S-shaped, which is typical of consecutive mechanisms with a buffer step or with parallel ones. Note that isotope responses $Z_{CO_2}(t)$ and $Z_{C_2H_4O}(t)$ are close in the character of approaching a new steady state. This means that slow relaxations for both reaction products are likely determined by the presence of a common buffer step. The observed isotope responses allowed us

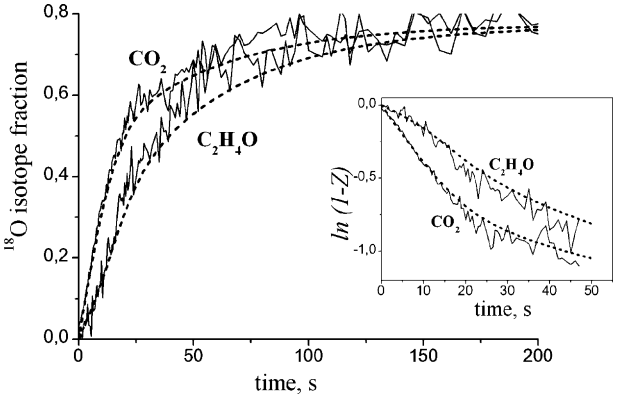

Fig. 5. The ^{18}O fraction in ethylene oxide and CO_2 after the $^{16}O_2$ replacement with $^{18}O_2$ in the feed gas (2.2% C_2H_4 + 1.2% O_2 + He) at $T = 180\,^{\circ}C$ and GHSV (Gas Hourly Space Velocity) = 3000 h^{-1} (solid lines—experiment; dotted lines—calculation). Inset: the logarithmic isotope responses for the same experiment.

to present the most probable mechanism as follows:

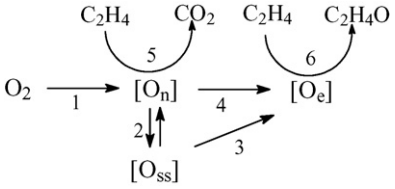

As was already noted, one of intermediate species identified is the subsurface oxygen [O_{ss}] not participating directly in the formation of reaction products. It is known that different surface oxygen species are involved in epoxidation and deep oxidation of ethylene. The [O_n] oxygen active in deep oxidation results from dissociative O_2 adsorption. Dissociative oxygen adsorption follows from the binominal distribution of CO_2 molecules in isotope composition [5]. Epoxidizing oxygen [O_e] forms from [O_n], directly (step (4)) or through subsurface oxygen (steps (2) and (3)). Modeling each pathway of [O_e] formation separately does not provide a satisfactory description of experimental responses. If [O_e] forms directly from [O_n], the calculated isotope responses $Z_{CO_2}(t)$ and $Z_{C_2H_4O}(t)$ virtually coincide. If the [O_e] formation proceeds only through subsurface oxygen, a shift of $Z_{C_2H_4O}(t)$ curve relative to $Z_{CO_2}(t)$ exceeds considerably the experimentally observed shift.

Thus, numerical analysis showed that the formation of epoxidizing oxygen [O_e] occurs simultaneously via two pathways with the rate ratio about 2:1. Subsurface oxygen easily exchanges with [O_n] adsorbed on the surface, and exchange rate is comparable to that of oxygen adsorption. One can also conclude from numerical modeling that the steps of [O_e] formation (steps 3 and 4) are almost irreversible, since the calculated curves $Z_{CO_2}(t)$ and $Z_{C_2H_4O}(t)$ reversibility of these steps.

Within the proposed reaction mechanism we estimated the concentrations of various adsorbed oxygen species (% monolayer):

$$1 < [O_n] < 5, \quad 0.5 < [O_e] < 3, \quad 120 < [O_{ss}] < 140,$$

as well as the rates of steps normalized per one oxygen atom (s^{-1}):

$$r_1 \approx 0.067, \quad r_2 \approx 0.044, \quad r_{-2} \approx 0.042, \quad r_3 \approx 0.001,$$

$$r_4 \approx 0.002, \quad r_5 \approx 0.064, \quad r_6 \approx 0.003.$$

Thus, it was proved that the concentrations of active oxygen species are very low and do not exceed several percents of a monolayer, i.e. practically all exchangeable oxygen is the subsurface one.

A molecule of ethylene is activated due to formation of its π-complex with Ag^+ cations [15,16]. The rates of epoxidation and deep oxidation can be written as follows:

$$r_6 = k_6\theta_\pi[O_e], \quad r_5 = k_5\theta_\pi[O_n] \tag{5}$$

The concentration θ_π was estimated from equilibrium constant of the π-complexes formation [15] and re-calculated for the given reaction conditions (T = 180 °C, $P_{ethylene}$ = 0.022 atm). Substituting the found values of $[O_n]$, $[O_e]$ and θ_π in (5), one can see that rate coefficients k_5 and k_6 have an order of 10^6–10^7 s^{-1}. It means that ethylene epoxidation and deep oxidation proceed very fast in the microsecond range. It is remarkable that despite of rather large response time of SSITKA setup measured by inert gas switching (*ca.* 1 s) it allows studying very fast reactions.

4.2. NO reduction with methane on Co-ZSM-5

The SSITKA study of selective NO reduction with methane included a study of labeled carbon transfer after the replacement of $^{12}CH_4$ with $^{13}CH_4$ in NO + O_2 + CH_4 + He flow as well as of labeled nitrogen and oxygen transfer after the replacement of $^{14}N^{16}O$ with $^{15}N^{18}O$ in NO + He, NO + O_2 + He and NO + O_2 + CH_4 + He flows in a plug-flow reactor. The Co-ZSM-5 catalyst containing 1.8% of cobalt as small oxide clusters was used [17].

The time dependencies of isotope fractions in NO and N_2 obtained after the stepwise replacement of ^{14}NO with ^{15}NO in the feed gas are shown on Fig. 6. One can see that N_2 response in logarithmic scale is convex down, which is typical of the mechanism with two parallel steps or the consecutive mechanism with a buffer step.

The study of the dynamics of ^{15}N isotope transfer under adsorption–desorption equilibrium (NO + O_2 + He) allowed us to reveal two types of NO_X complexes and to estimate their concentrations and formation rates depending on NO and O_2 concentrations [18]. According to *in situ* DRIFTS data, these complexes are assigned to nitrite–nitrate (1520 cm^{-1}) and $NO_2^{\delta+}$ species (2130 cm^{-1}) [17]. Note that nitrite–nitrates and $NO_2^{\delta+}$ differ clearly in the rates of their formation. Under the reaction conditions, the concentrations of both active species drop considerably. Therefore, it was proposed that the reaction occurs via two parallel pathways involving both active complexes. The rates of NO_X complexes interaction with methane were also calculated [19], and the reaction with participation of $NO_2^{\delta+}$ species was shown to proceed about 2.5 times faster than that of nitrite–nitrate ones. It was also found from the dynamics of ^{18}O label transfer that $NO_2^{\delta+}$ species form at the interface between CoO clusters and acid OH groups in zeolite (or at the paired Co^{2+}–OH sites). This agrees well with *in situ* DRIFTS data

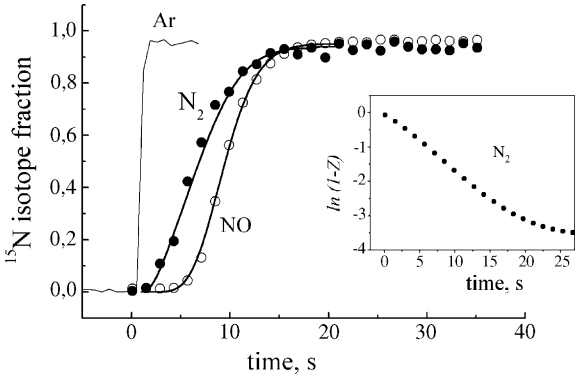

Fig. 6. The ^{15}N fraction in NO and N_2 after the ^{14}NO replacement with ^{15}NO in the feed gas (0.6% NO + 0.75% CH_4 + 3% O_2 + He) at T = 450 °C and GHSV = 15,000 h^{-1} (points—experiment; lines—calculation). Inset: the logarithmic isotope responses for the same experiment. The Ar response is presented as a reference.

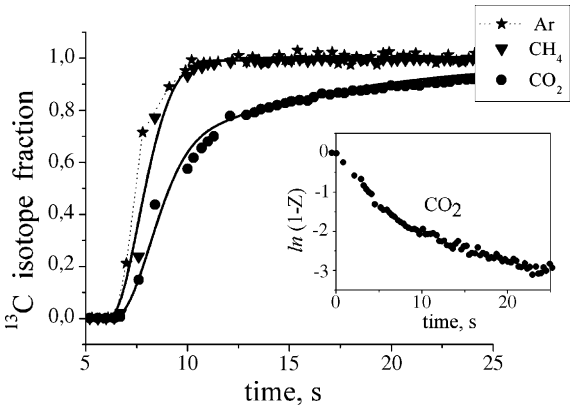

Fig. 7. The ^{13}C fraction in CH_4 and CO_2 after the $^{12}CH_4$ replacement with $^{13}CH_4$ in the feed gas (0.3% NO + 0.4% CH_4 + 3% O_2 + He) at T = 450 °C and GHSV = 36,000 h^{-1} (points—experiment; lines—calculation). Inset: the CO_2 logarithmic isotope response for the same experiment.

indicating that the $NO_2^{\delta+}$ formation correlates with a drop in the acid OH group band intensity [17].

Fig. 7 shows the methane and CO_2 isotope responses obtained after the $^{12}CH_4$ replacement with $^{13}CH_4$ in the feed gas. Again, as in the case of labeled nitrogen, the $Z^{13}_{CO_2}(t)$ dependence in logarithmic scale is convex down. The reaction mechanism including two parallel pathways of CH_4 conversion to CO_2 seems more favorable, since the formation of a large buffer of C-containing species (e.g. adsorbed methane) is hardly probable [20]. Moreover, numerical modeling of the ^{13}C transfer dynamics showed that the rate of fast (slow) CO_2 formation coincided well with the fast (slow) rates of $NO_2^{\delta+}$ (nitrite–nitrates) reaction with methane, respectively. In addition, the ratio between fast and slow rates of CO_2 formation (*ca.* 2.5) was very close to that estimated for adsorbed NO_X species. This ratio does not depend on the NO and methane concentration, but decreases with dropping of O_2 concentration in the feed gas [20].

Summarizing all the obtained data, we conclude that the selective NO reduction with CH_4 proceeds via parallel pathways involving different active sites:

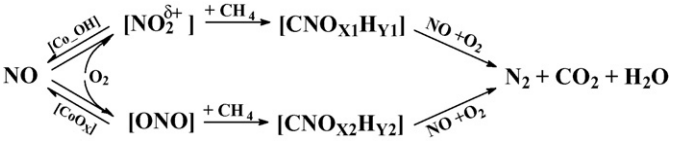

This mechanism includes the N_2 formation via two parallel pathways with participation of $NO_2^{\delta+}$ species located at the paired Co^{2+}–OH sites and nitrite–nitrate complexes formed on cobalt oxide clusters. It was shown that reaction turnover number (TON) over Co^{2+}–OH sites was *ca.* 20 times higher as compared to that over CoO_x. The isotope studies were carried out in a wide range of feed gas compositions and temperatures. This allowed us to find kinetic equations for the key reaction steps and to determine their rate coefficients and activation energies [18–20].

4.3. deNO$_X$ with propane accompanied by diffusion into the bulk of fiberglass catalyst

The transient isotopic technique (both experimental and modeling approaches) described above can be applied to investigate the kinetics of catalytic (chemical) reactions complicated by mass transfer processes. This was clearly demonstrated during the study of NO and water diffusion into the bulk of Pt-containing fiberglass

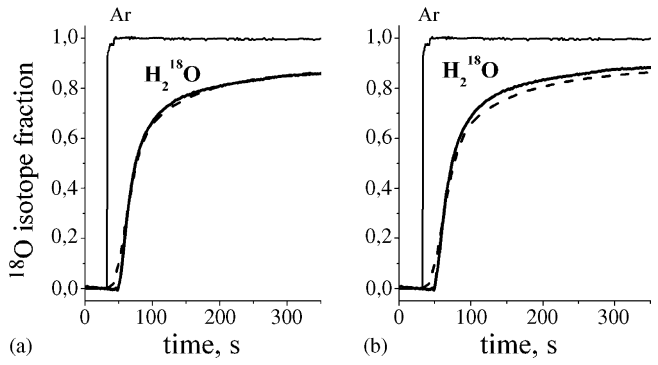

Fig. 8. The ^{18}O fraction in H_2O after the $H_2{}^{16}O$ replacement with $H_2{}^{18}O$ in the 1.6% H_2O + He flow at T = 400 °C and GHSV = 18,000 h^{-1} (solid lines—experiment, dotted lines—calculation). The sample is a fiberglass material with (a) and without (b) platinum.

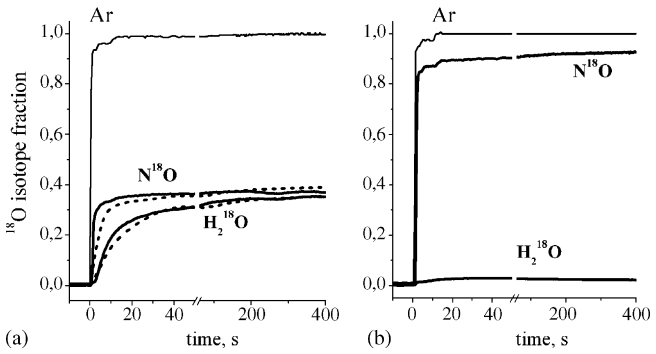

Fig. 9. The ^{18}O fraction in H_2O and NO after the $N^{16}O$ replacement with $N^{18}O$ in the 0.9% NO + 1.6% H_2O + He flow at T = 400 °C and GHSV = 18,000 h^{-1} (solid lines—experiment, dotted lines—calculation). The sample is a fiberglass material with (a) and without (b) platinum.

catalyst, which catalyzes NO reduction with propane. It was shown earlier that platinum is introduced into fiberglass as Pt small clusters (<10 Å) to a depth of *ca.* 10 nm [21]. Since these highly dispersed species are located in the fiberglass bulk, mass transfer of reacting molecules to active sites can have effect on reaction rate. Thus, both the polar reactant (NO) and the product (H_2O) diffusion into the bulk of fiberglass should be taken into account.

The isotope responses obtained after $H_2{}^{16}O$ replacement with labeled $H_2{}^{18}O$ are presented on Fig. 8. It is seen that fiberglass materials with and without platinum demonstrate almost the same ^{18}O responses. The simplest model of H_2O transfer into the fiberglass bulk plus isotope exchange with hydroxyls (r_1) was proposed [22]:

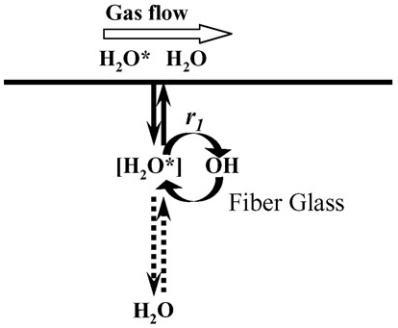

$$\frac{\partial \theta_{[H_2O]^*}}{\partial t} = D_{[H_2O]} \frac{\partial^2 \theta_{[H_2O]^*}}{\partial x^2} - r_1 (Z_{[H_2O]} - Z_{[OH]})$$

It is seen that this model describes well the experimental isotope responses. Within this model the total amount (concentration) of water plus hydroxyls and the H_2O diffusion coefficient were estimated as 100 μmol/g and 2×10^{-8} cm^2/s, respectively. The modeling of above process showed clearly that isotope substitution of OH groups in the bulk of glass matrix is limited by water diffusion.

Similar experiments on the $N^{16}O$ replacement with $N^{18}O$ in the feed gas containing both H_2O and NO were carried out (Fig. 9). In this case, the isotope responses obtained on catalyst with and without Pt differ substantially, indicating that NO interacts with a platinum species, which effectively participates in isotope exchange between NO and H_2O.

A model of NO and H_2O transfer into the fiberglass bulk and their oxygen exchange was also proposed:

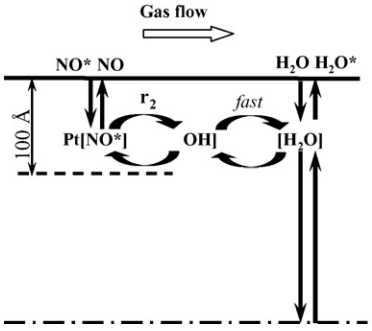

$$\frac{\partial \theta_{Pt[NO]^*}}{\partial t} = -r_2 (Z_{Pt[NO]} - Z_{[H_2O]})$$

$$\frac{\partial \theta_{[H_2O]^*}}{\partial t} = r_2 (Z_{Pt[NO]} - Z_{[H_2O]}) - D_{[H_2O]} \frac{4}{d} \left. \frac{\partial \theta_{[H_2O]^*}}{\partial x} \right|_{x=0}$$

where d—diameter of elementary fiber glass.

Basing on estimated above total amount of exchangeable hydroxyls and water (100 μmol/g) and rate of water diffusion in the fiberglass bulk, we estimated the concentrations of Pt[NO] species in the subsurface layers of fiberglass ($\theta_{Pt[NO]}$ = 3 μmol/g) and the rate of NO exchange with hydroxyls (r_2 = 10 μmol/g s). If the exchange rate is equal to rate of NO transfer from the gas phase to the fiberglass bulk (and back), one can estimate its mass transfer coefficient via gas–glass interface: $k = r_2/C_{NO}S \cong 2.5 \times 10^{-3}$ cm/s (where $S = 10^4$ cm^2/g is the specific surface area of fiberglass catalyst). Assuming that NO mass transfer in the bulk of fiberglass proceeds with the same rate as H_2O, we can estimate the characteristic time of diffusion $\tau_D = H^2/D_{H_2O} \sim 10^{-4}$ s, where

H = 10 nm is a depth of Pt location. Indeed, the NO diffusion in the bulk of glass matrix proceeds much faster than chemical reaction ($\tau_{isotope} = \theta_{NO}/r_{NO}$ = 0.3 s), e.g. mass transfer cannot limit the reaction rate.

5. Conclusions

It was demonstrated that SSITKA is a really powerful technique to identify the reaction mechanism and to estimate the surface concentrations of intermediates and reaction rate coefficients.

The ^{18}O isotope transfer dynamics in ethylene epoxidation on Ag showed that different oxygen species are involved in C_2H_4O and CO_2 formation. Epoxidizing oxygen is generated directly from non-selective nucleophilic one and through subsurface oxygen. The step of ethylene epoxidation itself was found to proceed extremely fast (in the microsecond range).

Three (^{13}C, ^{15}N and ^{18}O) labels were used to study the mechanism of NO reduction with CH_4 over Co-ZSM-5. It was shown that deNO_X proceeded via two parallel reaction pathways involving $NO_2^{\delta+}$ and nitrite–nitrate species formed at different active sites. The turnover frequency of the first pathway is 20 times higher than that of the second one.

The joint study of chemical reactions and mass transfer process into the bulk of Pt-containing fiberglass catalyst showed that diffusion of H_2O and, probably, NO molecules proceeds fast and cannot limit the reaction rate. The mass transfer parameters of NO and H_2O molecules were estimated.

Acknowledgements

Authors are grateful to L.G. Pinaeva, V.B. Goncharov (Boreskov Institute of Catalysis, Novosibirsk, Russia) and C. Mirodatos, A. van Veen (Institut de Recherches sur la Catalyse et l'environment de Lyon, Villeurbanne, France) for experimental support and fruitful discussion.

References

[1] J. Happel, Isotopic Assessment of Heterogeneous Catalysis, Academic Press, New York, 1986.
[2] P. Biloen, Transient kinetic methods, J. Mol. Catal. 21 (1983) 17–24.
[3] C. Mirodatos, Catal. Today 9 (1) (1991) 83–95.
[4] S.L. Shannon, J.G. Goodwin, Chem. Rev. 95 (3) (1995) 677–695.
[5] D.A. Bulushev, B.S. Bal'zhinimaev, Kin. Catal. 37 (1) (1996) 140–145.
[6] A.M. Efstathiou, X.E. Verykios, Appl. Catal. A 151 (1997) 109–166.
[7] K. Tamaru, Adv. Catal. 15 (1) (1964) 65–90.
[8] H. Kobayashi, M. Kobayashi, Catal. Rev. Sci. Eng. 10 (2) (1974) 139–176.
[9] C.O. Bennet, Catal. Rev. Sci. Eng. 13 (2) (1976) 121–148.
[10] M.I. Temkin, Adv. Catal. 28 (1979) 173–291.
[11] G.K. Boreskov, Adv. Catal. 15 (1964) 285–339.
[12] T. Yamada, T. Onishi, K. Tamaru, Surf. Sci. 133 (2) (1983) 533–546.
[13] E.M. Sadovskaya, D.A. Bulushev, B.S. Bal'zhinimaev, Kin. Catal. 40 (1) (1999) 54–61.
[14] P.G. Savva, A.M. Efstathiou, J. Catal. 257 (2008) 324–333.
[15] S.N. Goncharova, E.A. Paukshtis, B.S. Bal'zhinimaev, Appl. Catal. A 126 (1) (1995) 67–84.
[16] B.S. Bal'zhinimaev, Kin. Catal. 40 (6) (1999) 795–810.
[17] L.G. Pinaeva, E.M. Sadovskaya, A.P. Suknev, V.B. Goncharov, V.A. Sadykov, B.S. Balzhinimaev, T. Decamp, C. Mirodatos, Chem. Eng. Sci. 54 (1999) 4327–4335.
[18] E.M. Sadovskaya, A.P. Suknev, L.G. Pinaeva, V.B. Goncharov, B.S. Bal'zhinimaev, C. Chupin, C. Mirodatos, J. Catal. 201 (2001) 159–168.
[19] E.M. Sadovskaya, A.P. Suknev, L.G. Pinaeva, V.B. Goncharov, B.S. Bal'zhinimaev, C. Chupin, J. Perez-Ramirez, C. Mirodatos, J. Catal. 225 (2004) 179–189.
[20] E.M. Sadovskaya, A.P. Suknev, V.B. Goncharov, B.S. Bal'zhinimaev, C. Mirodatos, Kin. Catal. 45 (3) (2004) 436–445.
[21] L.G. Simonova, V.V. Barelko, A.V. Toktarev, V.I. Zaikovskii, V.I. Bukhtiyarov, V.V. Kaichev, B.S. Bal'zhinimaev, Kin. Catal. 42 (6) (2001) 837–846.
[22] E.M. Sadovskaya, A.P. Suknev, A.V. Toktarev, L.G. Simonova, E.A. Paukshtis, B.S. Bal'zhinimaev, Kin. Catal. 47 (1) (2006) 131–137.